Whole-brain computational modeling reveals disruption of microscale brain dynamics in HIV infected individuals

Yuchuan Zhuang [a], Zhengwu Zhang [b,c] , Madalina Tivarus [d,c] , Xing Qiu [b] , Jianhui Zhong [d,e,*] , Giovanni Schifitto [f,d,*]

[a] Department of Electrical and Computer Engineering, University of Rochester, 500 Computer Studies Building, Rochester, New York 14627, USA

[b] Department of Biostatistics and Computational Biology, University of Rochester Medical Center, 265 Crittenden Boulevard, CU 420630, Rochester, New York 14642, USA

[c] Department of Neuroscience, University of Rochester Medical Center, 601 Elmwood Avenue, KMRB G.9602, Rochester, New York 14642, USA

[d] Department of Imaging Sciences, University of Rochester Medical Center, 601 Elmwood Ave, Rochester, New York 14642, USA

[e] Department of Biomedical Engineering, University of Rochester, 201 Robert B. Goergen Hall, Rochester, New York 14627, USA

[f] Department of Neurology, University of Rochester Medical Center, 601 Elmwood Avenue, Rochester, New York 14642, USA

*Corresponding authors: Dr. Jianhui Zhong, 601 Elmwood Ave, Rochester, University of Rochester Medical Center, New York 14642, USA, E-mail address: Jianhui_Zhong@URMC.Rochester.edu

Dr. Giovanni Schifitto, 601 Elmwood Ave, Rochester, University of Rochester Medical Center, New York 14642, USA, E-mail address: Giovanni_Schifitto@URMC.Rochester.edu

1. Supplementary Methods

1.1. Preprocessing of resting-state fMRI

The preprocessing of fMRI using FEAT(Jenkinson et al., 2012) including head motion correction carried by MCFLIRT (Jenkinson et al., 2002) using rigid-body registration to the reference image; B0 inhomogeneity correction using boundary-based registration (BBR) with a fieldmap and registration to T1w image; slice timing correction; brain extraction using BET (Smith, 2002); spatial smoothing using a Gaussian kernel with full width at half maximum (FWHM) of 5 mm; and linear trend removal by applying a high-pass temporal filtering. The T1w image was warped to a 2mm MNI standard space using FNIRT, and coregistered with the rsfMRI using linear transformation, yielding a functional image resampled in 2mm MNI standard space. MELODIC option was switched on to prepare for FIX, an ICA-based noise removal.

1.2. Simulated FC using rMFM model

The MFM model was derived from a detailed spiking brain model (Deco and Jirsa, 2012), where each brain region is modeled by a spiking attractor network, represented by two pools of neuron populations: a population of excitatory pyramidal neurons and a population of GABAergic inhibitory neurons. Within each brain region, the excitatory neurons and the inhibitory neurons are fully connected, the strength of this intra-region connection defined as recurrent connection strength w. The inter-region connections are weighted by the structural connectivity strength C_{ij} multiplied by a global scaling factor G. MFM uses the dynamic mean field reduction of each local spiking attractor (Wong and Wang, 2006), to simplify the mathematical description of the spiking model while fairly approximating the dynamics of the spiking network (Deco et al., 2013). The improved MFM, rMFM, relaxes the recurrent connection strength w and subcortical inputs I in the MFM model, so that each brain region has different values of recurrent connection strength w_i and subcortical inputs I_i. The rMFM within each brain region can be modeled using a set of coupled nonlinear stochastic differential equations, Eq. (1-3):

$$\frac{dS_i(t)}{dt} = -\frac{S_i}{\tau_s} + \gamma(1 - S_i)H(x_i) + \sigma v_i(t) \quad (1)$$

$$H(x_i) = \frac{ax_i - b}{1 - \exp\big(-d(ax_i - b)\big)} \quad (2)$$

$$x_i = w_i J S_i + GJ \sum_j C_{ij} S_j + I_i \quad (3)$$

where S_i, $H(x_i)$, and x_i denote the average synaptic gating variable, the population firing rate, and the total input current at i-th brain region respectively, C_{ij} is the streamline counts connecting i-th brain region and j-th brain region, representing the anatomical connection strengths between brain areas i and j, w_i is the recurrent connection strength at i-th brain region and I_i is the excitatory subcortical input at i-th brain region. Here the total input current at i-th brain region x_i is driven by incoming local recurrent inputs within the same cortical area $w_i J S_i$, long range inputs from all other cortical area $GJ \sum_j C_{ij} S_j$, and subcortical inputs I_i. The inter-areal connections are weighted by the structural connectivity strength C_{ij}. Parameter values for the input output function $H(x_i)$ are a = 270(VnC), b =1008(Hz), and d = 0.154(s); the kinetic parameters are $\gamma = 0.641$, $\tau_s = 100$ms; the synaptic couplings are J = 0.2609(nA); $v_i(t)$ is the uncorrelated standard Gaussian noise and σ is the noise amplitude. These values are derived from Deco et. al (Deco et al., 2013).

Simulated BOLD time series were derived from the simulated neuronal activities using the Ballon-Windkessel hemodynamic model (Friston et al., 2000; Friston et al., 2003), which describes BOLD signal as a function of changes in neuronal activity, cerebral blood flow, cerebral blood volume, and deoxyhemoglobin content, represented by Eq.(4-7). In brief, for the i-th brain region, neuronal activity S_i causes an increase in a vasodilatory signal z_i, which results in an increase in inflow f_i, with concomitant changes in blood volume v_i and deoxyhemoglobin content q_i.

$$\frac{\partial z_i(t)}{\partial t} = S_i - \kappa z_i - \gamma(f_i - 1) \quad (4)$$

$$\frac{\partial f_i(t)}{\partial t} = z_i \tag{5}$$

$$\tau \frac{\partial v_i(t)}{\partial t} = f_i - {v_i}^{1/\alpha} \tag{6}$$

$$\tau \frac{\partial q_i(t)}{\partial t} = \frac{f_i}{\rho}\left[1 - (1 - \rho)^{1/f_i}\right] - q_i {v_i}^{1/\alpha - 1} \tag{7}$$

where $\kappa = 0.65$ per s is the rate of signal decay, $\gamma = 0.41$ per s is the rate of flow-dependent elimination, $\tau = 0.98$ is the hemodynamic transit time, $\rho = 0.34$ is the resting oxygen extraction fraction and $\alpha = 0.32$ is the Gubb's exponent (Grubb et al., 1974). BOLD signal for each brain area was estimated by Eq. (8).

$$BOLD_i = V_0[k_1(1 - q_i) + k_2(1 - q_i/v_i) + k_3(1 - v_i)] \tag{8}$$

where V_0 = 0.02 is the resting blood volume fraction, and k_1, k_2, and k_3 are parameters dependent on field strength, calculated by following Eq.(9-11) below, revised from the Buxton model (Buxton et al., 1998) as in (Stephan et al., 2007; Heinzle et al., 2016).

$$k_1 = 4.3 v_0 E_0 TE \tag{9}$$

$$k_2 = \varepsilon r_0 E_0 TE \tag{10}$$

$$k_3 = 1 - \varepsilon \tag{11}$$

where $v_0 \cong 28.265 \cdot B_0$ is the frequency offset at the outer surface of magnetized vessels and depends linearly on the main magnetic field strength B_0, which is 3T in our case; $r_0 \cong 110$ Hz in a 3T MR scanner, is the intravascular relaxation rate as a function of oxygen saturation; $\varepsilon = S_I/S_E \cong 0.47$ represents the ratio between intravascular and extravascular MR signal.

The simulated neuronal activity and BOLD time series for each brain region were numerically integrated using Euler's method. The length of the simulated BOLD time series was 7 minutes, with the first 2 minutes discarded to allow model activity and simulated fMRI

signal to stabilize (Schirner et al., 2018). The BOLD signal was down sampled to 2 second to match our empirical rsfMRI imaging protocol.

1.3. Graph theoretical measurements calculation

Mean clustering coefficient: the clustering coefficient for each node implies network segregation (Watts and Strogatz, 1998; Rubinov and Sporns, 2010). The mean clustering coefficient is the average clustering coefficient across all nodes, which can be calculated with Eq.(12).

$$C = \frac{1}{n}\sum_{i\in N} C_i = \frac{1}{n}\sum_{i\in N} \frac{2t_i}{k_i(k_i-1)} \tag{12}$$

where C_i is the clustering coefficient of node i ($C_i = 0$ for $k_i < 2$), k_i is the degree of node i meaning the number of links connected to the node, t_i is the number of closed triangles.

Characteristic path length: the mean shortest path length between all pairs of brain regions is calculated with Eq.(13).

$$L = \frac{1}{n}\sum_{i\in N} L_i = \frac{1}{n}\sum_{i\in N} \frac{\sum_{i\in N, j\neq i} d_{ij}}{n-1} \tag{13}$$

where d_{ij} is the shortest path length between nodes i and j. L_i is the average distance between node i and all other nodes.

Global efficiency: efficiency between two nodes is the inverse of the shortest path length between these brain regions. Global efficiency (Latora and Marchiori, 2001; Rubinov and Sporns, 2010) of the network is the average efficiency for all node pairs, and is calculated with Eq. (14).

$$E = \frac{1}{n}\sum_{i\in N} E_i = \frac{1}{n}\sum_{i\in N} \frac{\sum_{i\in N, j\neq i} d_{ij}^{-1}}{n-1} \quad (14)$$

where E_i is the efficiency of node i.

Network smallworldness: when the network is highly clustered, while it has approximately the same characteristic path length as random networks (Watts and Strogatz, 1998; Rubinov and Sporns, 2010), it's considered as a small-world network. And it can be characterized by a single measurement, network smallworldness (Humphries and Gurney, 2008), as calculated with Eq. (4).

$$S = \frac{C/C_{rand}}{L/L_{rand}} \quad (15)$$

where C and C_{rand} are the clustering coefficients, and L and L_{rand} are the characteristic path length of the respective tested network and a random network.

To further investigate the relationship between the microscale brain dynamics derived from rMFM model and the topological properties, we also calculated the nodal clustering coefficient C_i in Eq (12), local efficiency E_i in Eq (14) for the FC in the training dataset for the 68 nodes in Desikan atlas for each group (the results for Destrieux atlas are reported in supplementary materials).

2. Supplementary Results

2.1. Age matching in training and test groups.

Supplementary Table 1. Mean and standard deviation of age in training and test groups

	Training group (subject number)	Test group (subject number)
Healthy Control (HC)	37.73±13.31 (n=22)	37.52±12.35 (n=21)
HIV+ Baseline (HIV+BSL)	35.83±13.66 (n=23)	35.74±12.09 (n=23)
HIV+ 12-week (HIV+12wk)	36.63±13.34 (n=16)	36.44±14.51 (n=16)

2.2. FC simulation results using rMFM

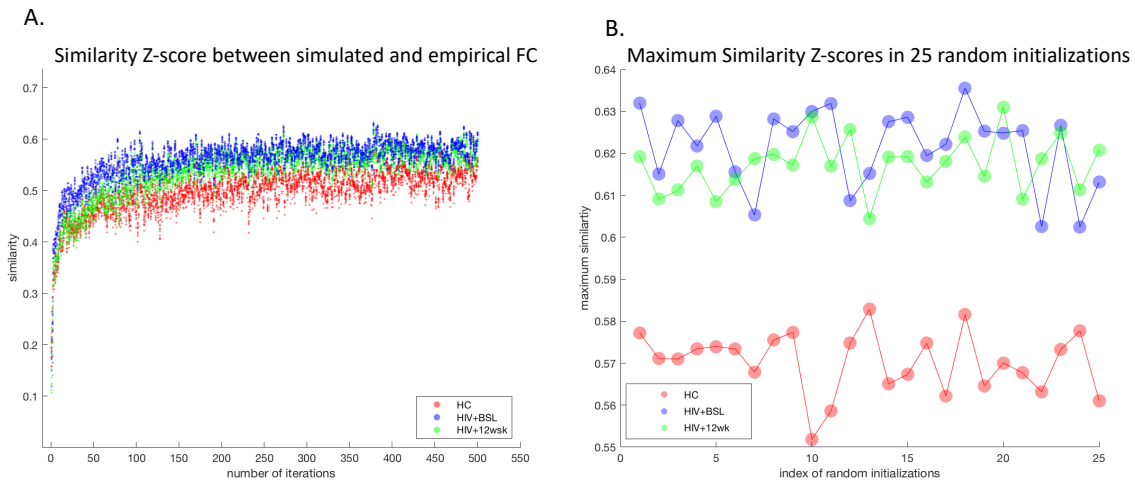

Supplementary Fig. 1. rMFM optimization results**.** rMFM model parameter estimations for HC (red), HIV+BSL (blue), and HIV+12wk(green). A). the similarity values between simulated FC and empirical FC changes across 500 iterations. The model estimation is improved across 500 iterations for each cohort. Each dot represents the similarity value between simulated FC and empirical FC. The recurrent connection strength w , and subcortical input strength I were updated after each iteration. B). the maximum similarity changed across 25 random initializations for each cohort. Each dot represents the maximum similarity value after 500 iterations; the rMFM model parameters corresponding to this maximum similarity value were recorded. For each cohort, we run the rMFM modeling using

25 different random initialization parameters, which yielded a total of 75 simulations. Red: HC, Blue: HIV+BSL, Green: HIV+12wk.

In Supplementary Fig. 1A, each dot represents the similarity value, calculated as the Pearson's correlation between the simulated FC and empirical FC after each iteration. The similarity value increased dramatically (simulated FC converging to the empirical FC) in the first 100 iterations, and then plateaued after 250 iterations. Supplementary Fig. 1A shows that 500 iterations are sufficient for the purpose of model optimization. After 500 iterations were completed, we extracted the maximum similarity and its corresponding rMFM model parameters. We repeated this step with 25 different random initializations for each cohort, the maximum similarity Z-scores of each random initializations are shown in Supplementary Fig. 1B.

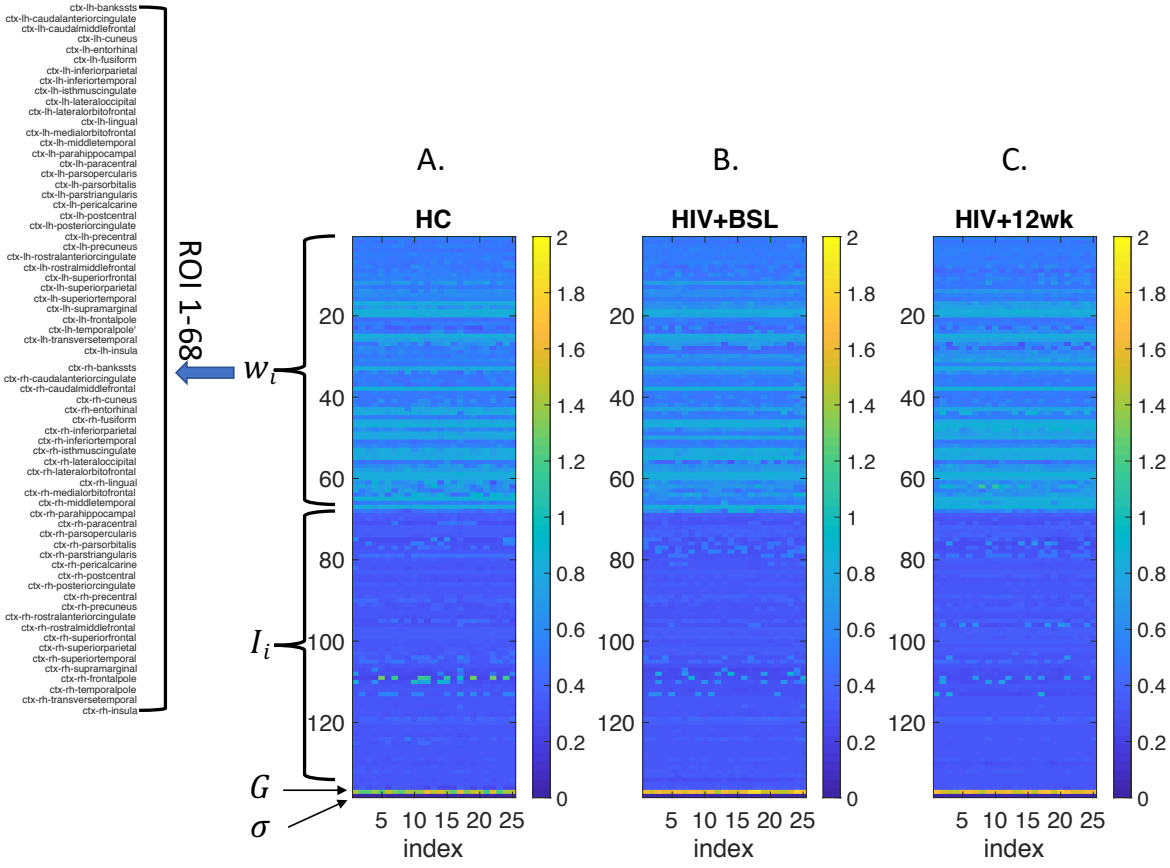

Supplementary Fig. 2. rMFM model parameters. rMFM model parameters across different randomized initialization parameters for each cohort, A). HC. B). HIV+BSL, C). HIV+12wk. Each plot is a 138x25 matrix. Each column represents the optimized rMFM model parameters after 500 iterations using 1 random initialization. We used 25 different random

initializations for each cohort, yielding 25 columns in each plot. The first 68 rows indicate w_i -recurrent connection strength for 68 ROIs, second 68 rows indicate I_i – subcortical strength for 68 ROIs. The 137th row indicates the G-global scaler, and the 138th row indicates the σ – amplitude of gaussian noise.

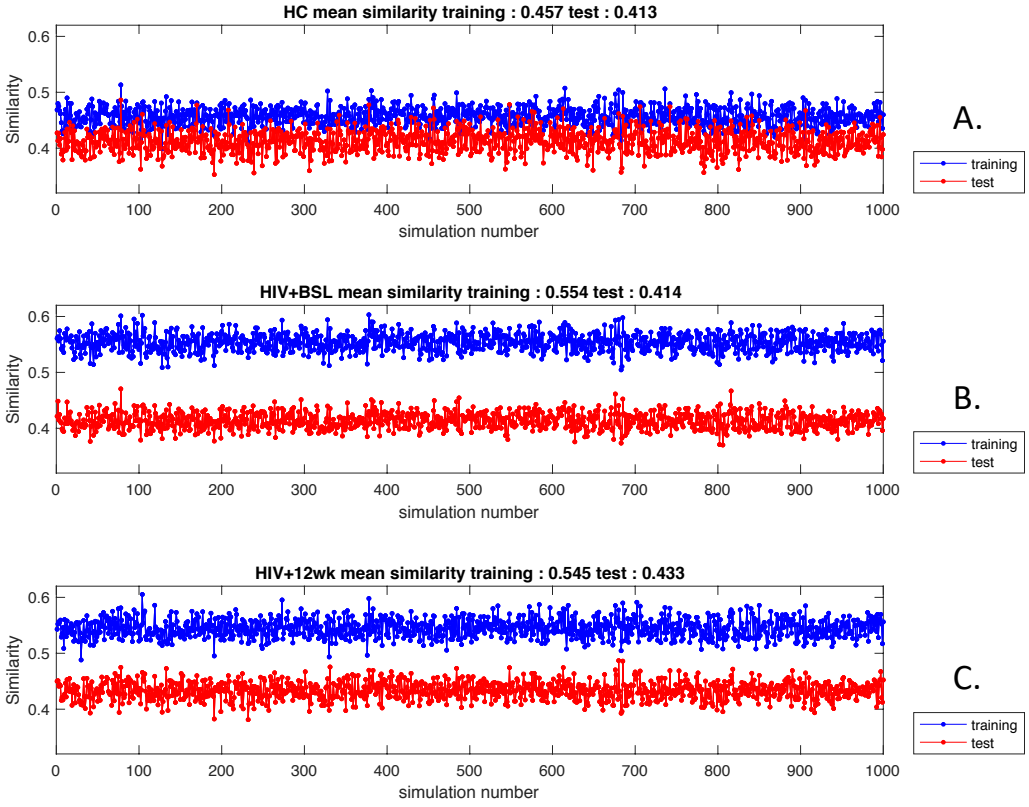

Supplementary Fig. 3. rMFM model validation results. rMFM model validations using test datasets for HC, HIV+BSL, and HIV+12wk. The three plots from top to bottom are similarity results for HC, HIV+BSL, and HIV+12wk respectively. The blue dots and line are the similarity results using training datasets across 1000 simulations, while the red dots and line are the similarity results using testing datasets across 1000 simulations.

Supplementary Fig. 3 indicates the similarity results of simulated FC and empirical FC through 1000 simulations using test dataset. The averaged similarity values for each cohort for the test datasets are 0.413, 0.414, and 0.433 respectively. For each cohort, the simulation results using the test dataset decreased 0.044-0.140 compared with simulation using training dataset, but still relatively high (above 0.41) indicating a good rMFM estimation.

2.3. Local brain dynamic properties changes

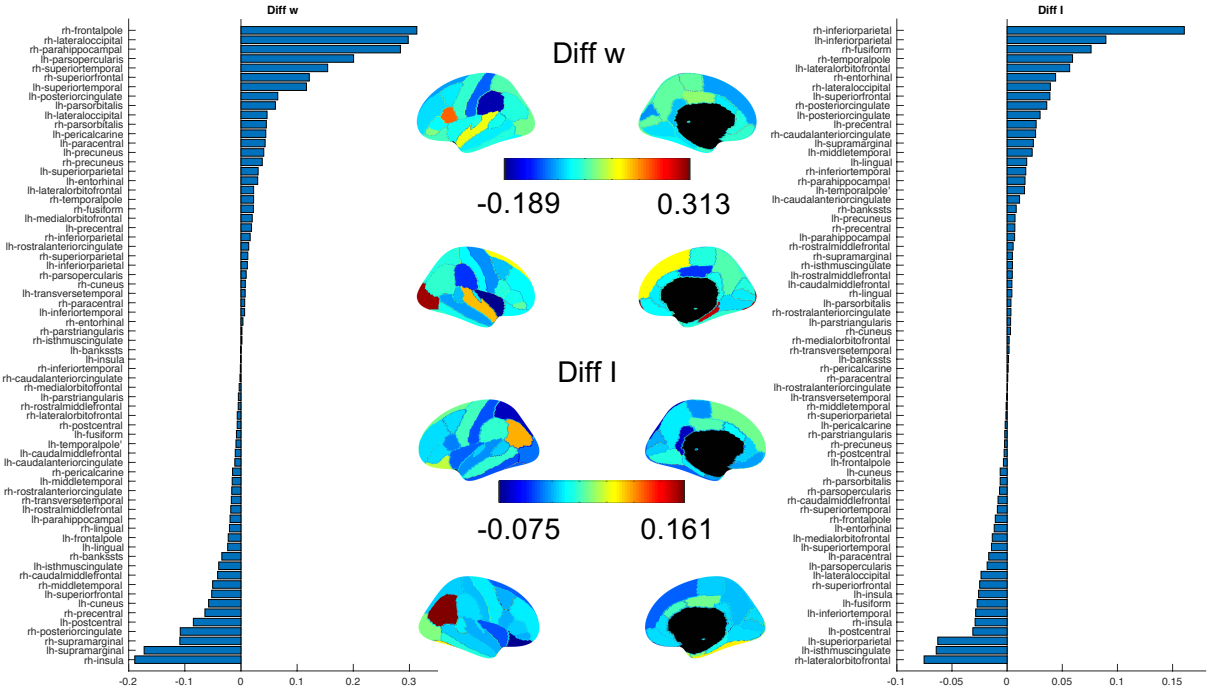

Supplementary Fig. 4. Ranked differences of whole-brain rMFM model parameters, recurrent connection strengths *w* (left), and subcortical inputs *I* (right) for each brain region. First column: regional recurrent connection strength difference between HIV+BSL and HC, sorted by the difference (diff = HC – HIV+BSL). Second column: the difference of *w*, and *I* were mapped on the brain surface, indicating the anatomical locations. Hotter color towards red means HC is greater than HIV+BSL, cooler color towards blue means HC is smaller than HIV+BSL. Third column: regional subcortical inputs difference between HIV+BSL and HC, sorted by the difference.

Supplementary Fig. 4 shows the difference of rMFM model parameters between HIV+BSL and HC, sorted by the difference (diff = HC – HIV+BSL) of recurrent connection strength w, and subcortical inputs I. The brain plots color-coded the difference between HC and HIV+BSL. The hotter regions indicate the rMFM model parameters are greater in HC, while the cooler regions indicate the values are greater in HIV. The highest differences of recurrent connections between HC and HIV+BSL were found in right frontal pole, right lateral occipital lobe, right parahippocampal gyrus, right insula, right supramarginal gyrus, and left supramarginal gyrus. The highest differences of subcortical input strength between HC and

HIV+BSL were found in right inferio parietal lobule, left inferio parietal lobule, right fusiform, right lateral orbitofrontal, left isthmus of the cingulate gyrus, and left superioparietal lobule. These results also indicate that the HIV-infection altered the local cortical dynamics in the brain, so we only calculate the difference between HC and HIV+BSL in this analysis.

2.4. rMFM model validation

We further validated the rMFM estimation using a different training /test dataset for each cohort, and also run the model optimization with 500 and 1000 iterations, using 10~15 different initial parameters to further validate our model. Supplementary Fig. 5 A and B show the model optimization results after 500 iterations, Supplementary Fig. 5 C and Supplementary Fig. 5 D show the results after 1000 iterations. The plateau appears around 250 iterations for both cases, indicating 500 iterations of model parameter estimation is a good number to get a satisfactory and stable simulated FC. The maximum similarity values are in the range of 0.5 to 0.65, which were the same as previous results. Supplementary Fig. 5E and Supplementary Fig. 5F are calculated from the rMFM of validation test datasets with 500 iterations.

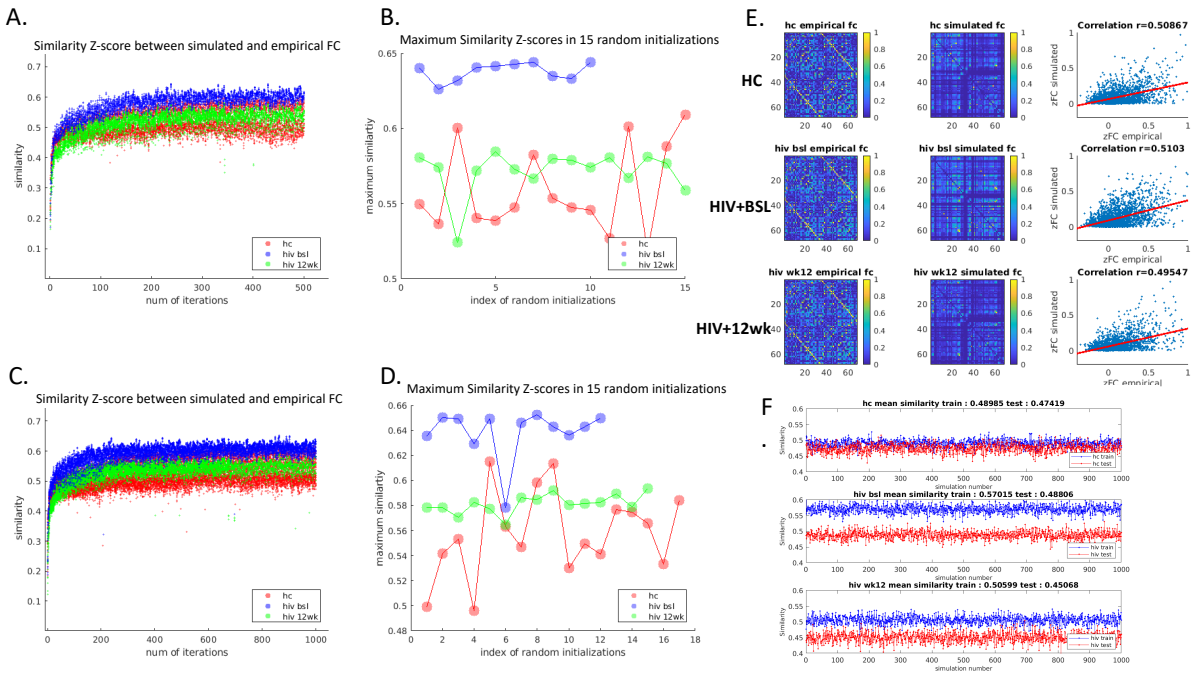

Supplementary Fig. 5. rMFM model validation. A) the similarity values between simulated FC and empirical FC changes across 500 iterations. B). the maximum similarity changed

across different random initializations for each cohort. C) the similarity values between simulated FC and empirical FC changes across 1000 iterations. D). the maximum similarity changed across different random initializations for each cohort across 1000 iterations. E) rMFM models generated simulated FC for HC, HIV+BSL, and HIV+12wk, respectively. F) rMFM model validations. The three plots from top to bottom are similarity results for HC, HIV+BSL, and HIV+12wk respectively. The blue dots and line are the similarity results using training datasets across 1000 simulations, while the red dots and line are the similarity results using test datasets across 1000 simulations.

2.5. Neuropsychological test score

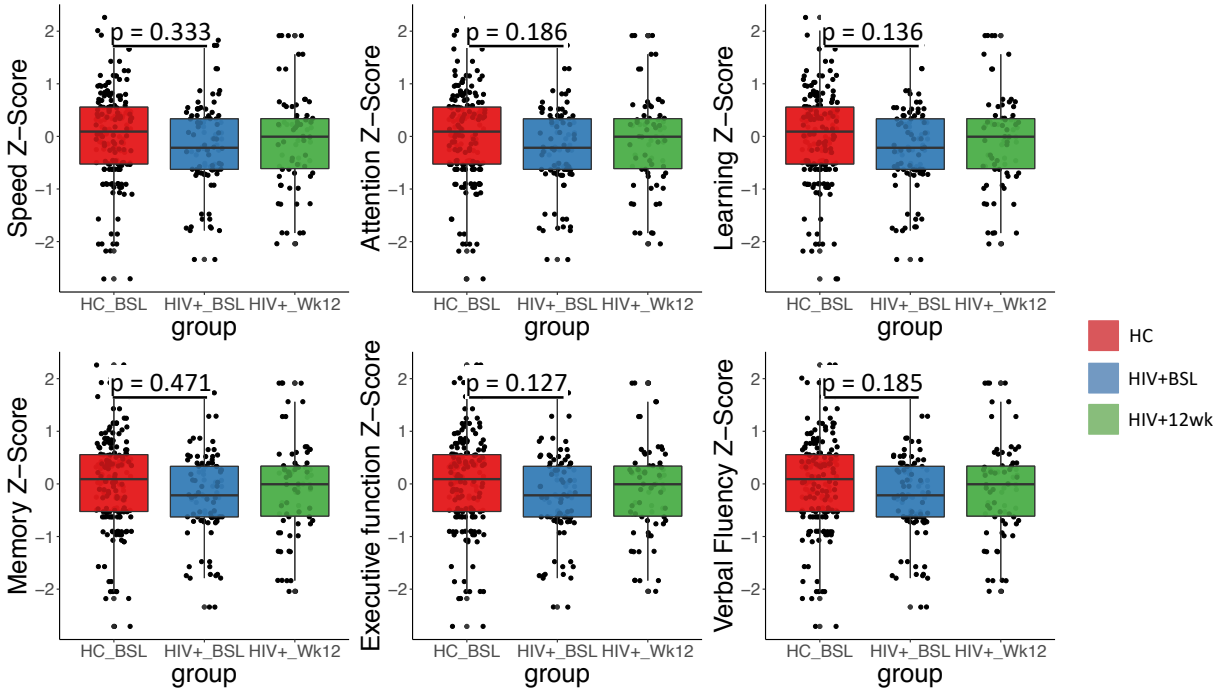

Supplementary Fig. 6 Neuropsychological test z-score for other cognitive domains: Speed of information process, attention, learning, memory, executive function, and verbal fluency Z-score. No significant difference was found between HIV+BSL and HC (uncorrected p>0.1).

2.6. rMFM modeling results using Destriuex atlas

We also replicated the rMFM model simulation using a finer parcellated atlas, the Destriuex atlas. The simulation results can be found in Supplementary Fig. 7. The rMFM simulation performed well on a finer segmented atlas. The similarities across 20 random initializations are within 0.54-0.61. The simulated FC and empirical FC in the test dataset also worked well,

see Supplementary Fig. 5, yielding similarities are 0.439, 0.392, and 0.447 for HC, HIV+BSL, and HIV+12wk, respectively.

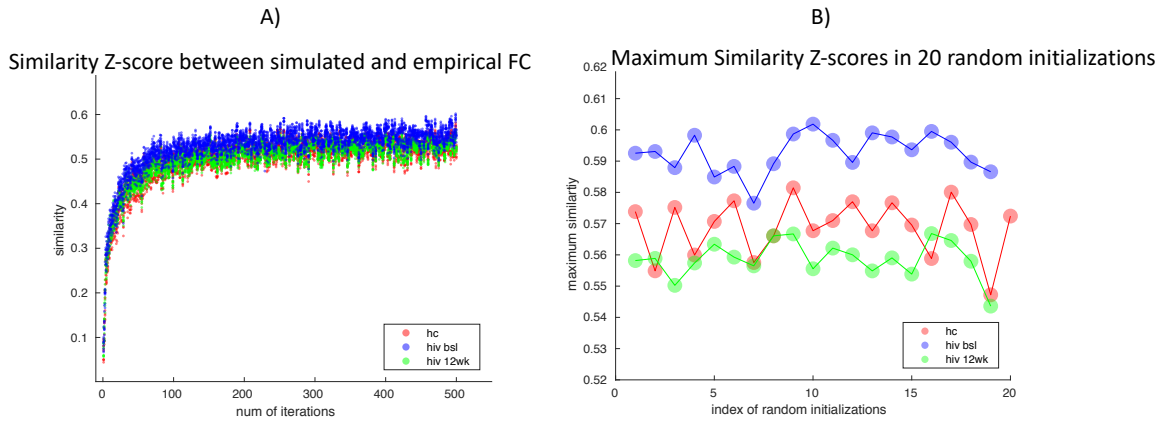

Supplementary Fig. 7. Validation the rMFM model parameter estimations using Destrieux atlas for HC (red), HIV+BSL (blue), and HIV+12wk(green). A). the similarity values between simulated FC and empirical FC changes across 500 iterations. The model estimation is improved across 500 iterations for each cohort. Each dot represents the similarity value between simulated FC and empirical FC. The recurrent connection strength w , and subcortical input strength I were updated after each iteration. B). the maximum similarity changed across 20 random initializations for each cohort. Each dot represents the maximum similarity value after 500 iterations; the rMFM model parameters corresponding to this maximum similarity value were recorded. For each cohort, we run the rMFM modeling using 20 different random initialization parameters, which yielded a total of 60 simulations. Red: HC, Blue: HIV+BSL, Green: HIV+12wk.

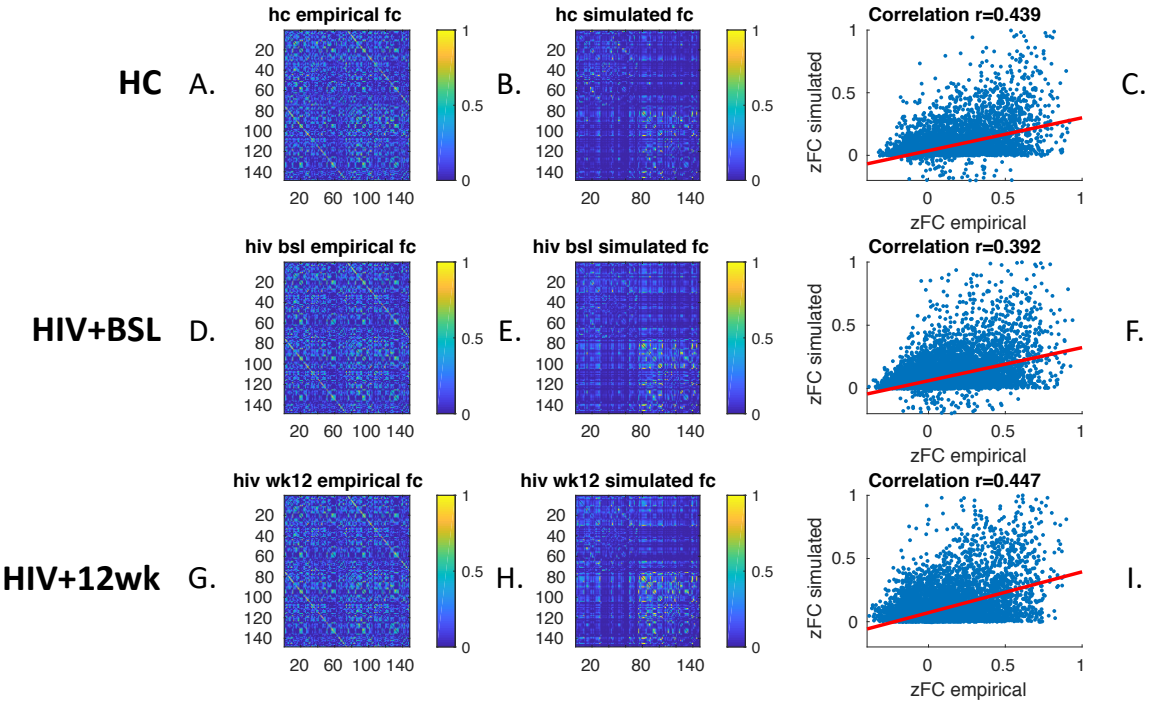

Supplementary Fig. 8. rMFM models generated the simulated FC for HC, HIV+BSL, and HIV+12wk, respectively using Destrieux atlas. Left column A) D) G): the averaged empirical FC in test dataset for each cohort. Middle column B) E) H): the averaged simulated FC. Right column C) F) I): The correlation between empirical and simulated FC.

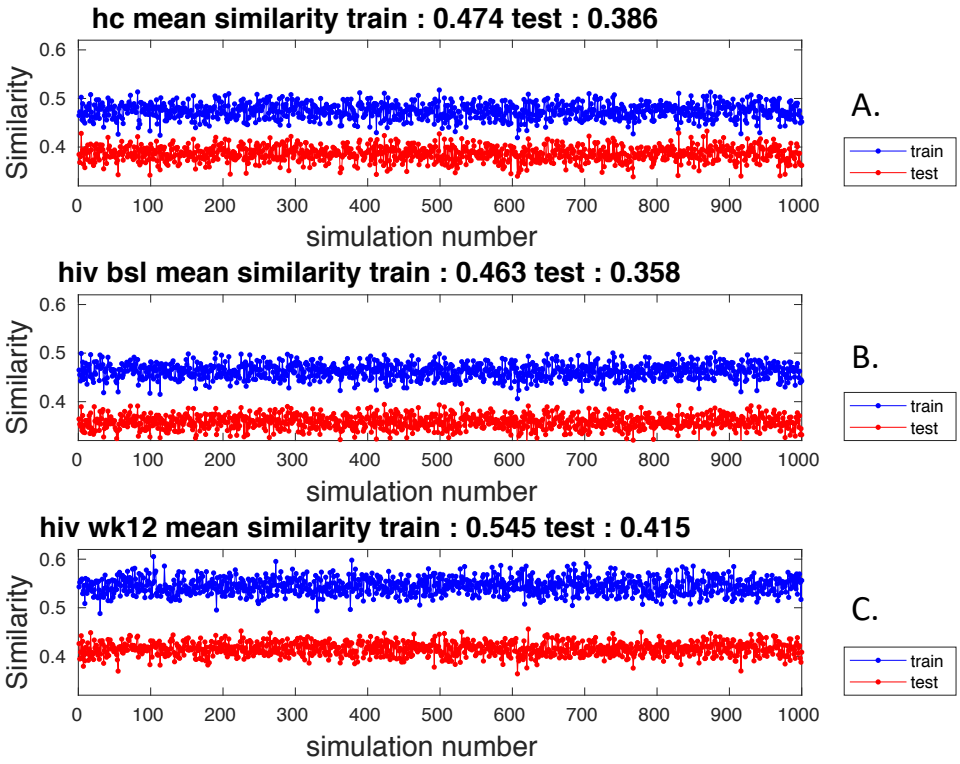

Supplementary Fig. 9. rMFM model validations using Destrieux atlas, using test datasets. The three plots from top to bottom are similarity results for HC, HIV+BSL, and HIV+12wk respectively. The blue dots and line are the similarity results using training datasets across 1000 simulations, while the red dots and line are the similarity results using testing datasets across 1000 simulations.

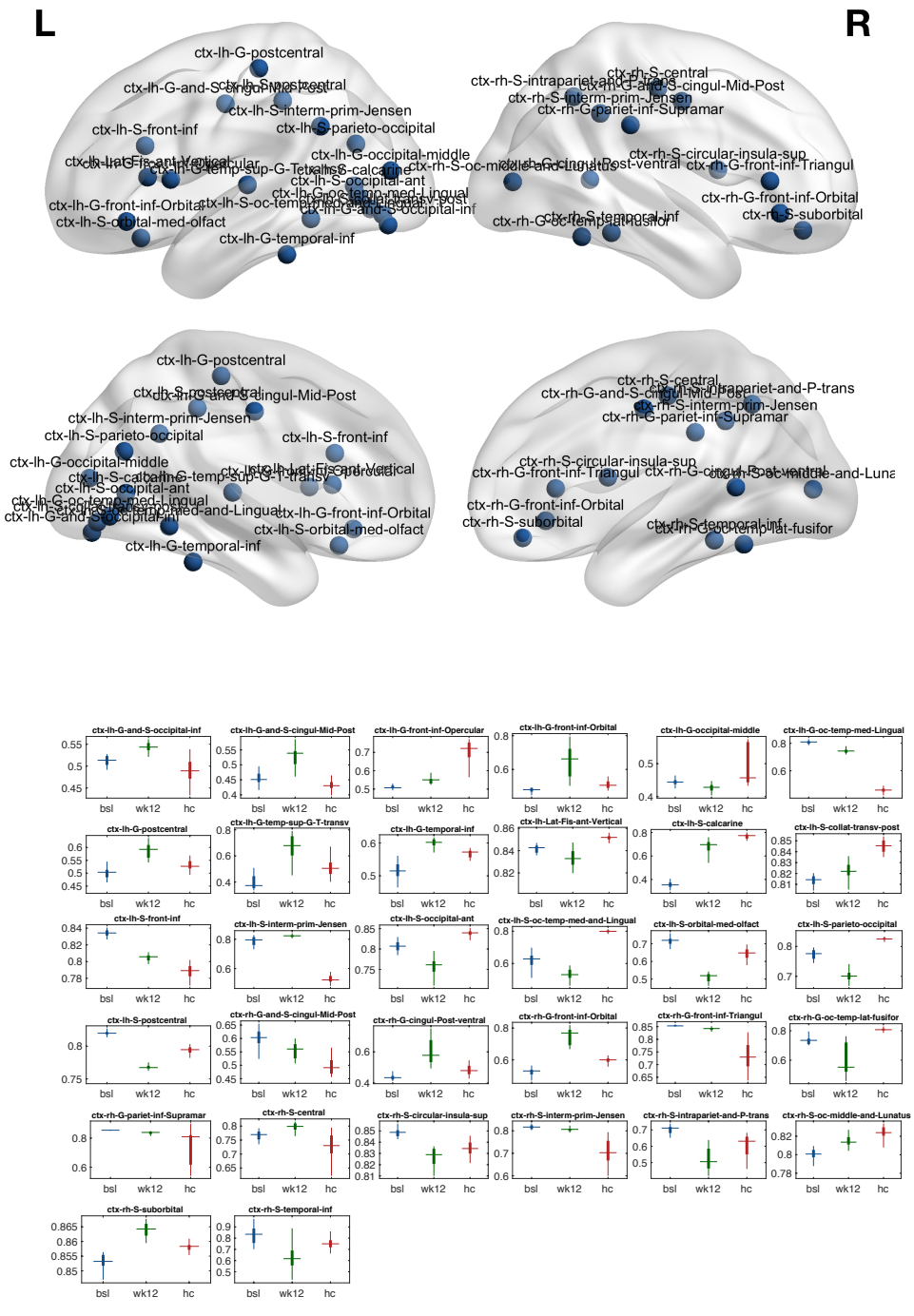

Supplementary Fig. 10. The regional recurrent connection strengths results using Destrieux atlas. Top: the regional recurrent connection changes in these nodes plotted on a smoothed brain surface indicate their anatomical location. Bottom: bar plots show the recurrent connection strength for each ROIs. Red: HC, Blue: HIV+BSL, Green: HIV+12wk.

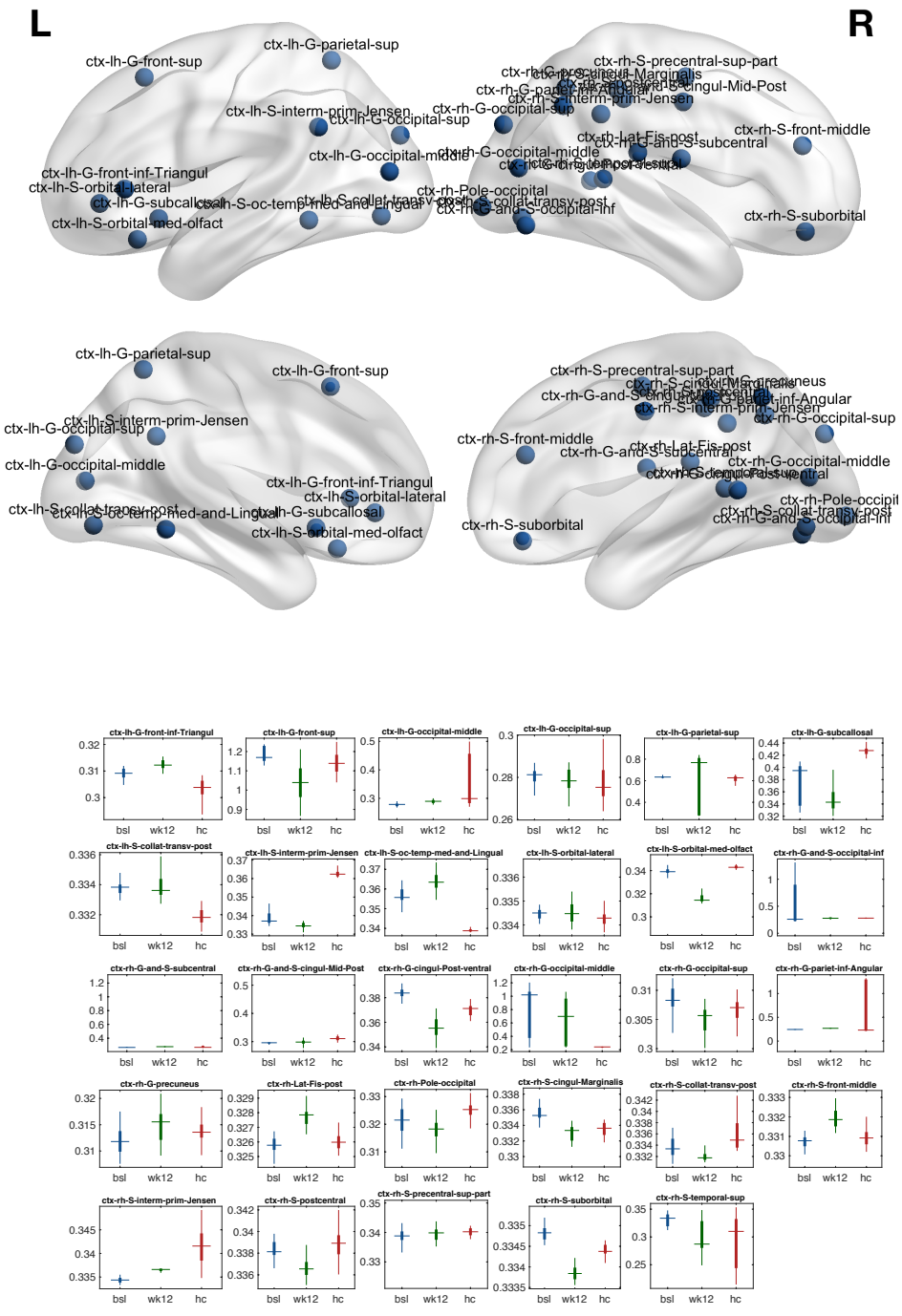

Supplementary Fig. 11. The subcortical input strengths results using Destrieux atlas. Top the subcortical inputs change in these nodes plotted on a smoothed brain surface indicate their anatomical location. Bottom: bar plots show the recurrent connection strength for each ROIs. Red: HC, Blue: HIV+BSL, Green: HIV+12wk.

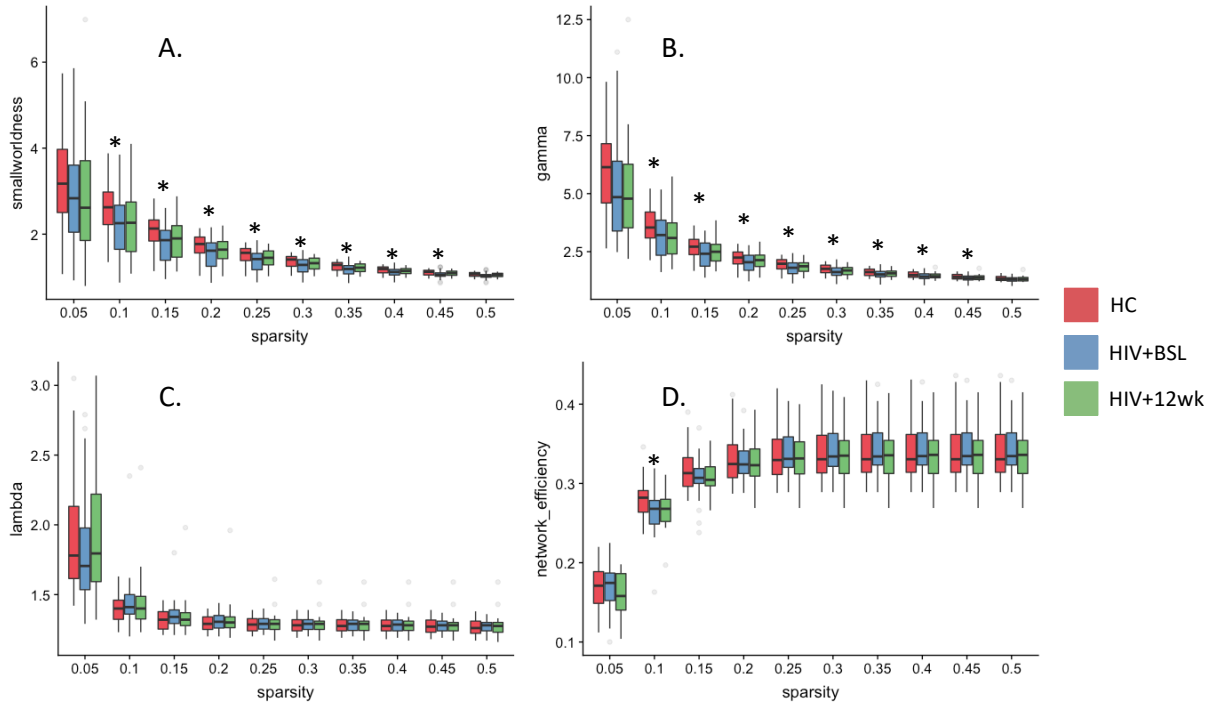

Supplementary Fig. 12. Graph theoretical measurements on weighted functional connectivity matrix across network sparsity range from 0.05 to 0.5. A). smallworldness. B). global clustering coefficient. C). global characteristic path length. D). global network efficiency. * FDR corrected p<0.05. Red: HC, Blue: HIV+BSL, Green: HIV+12wk.

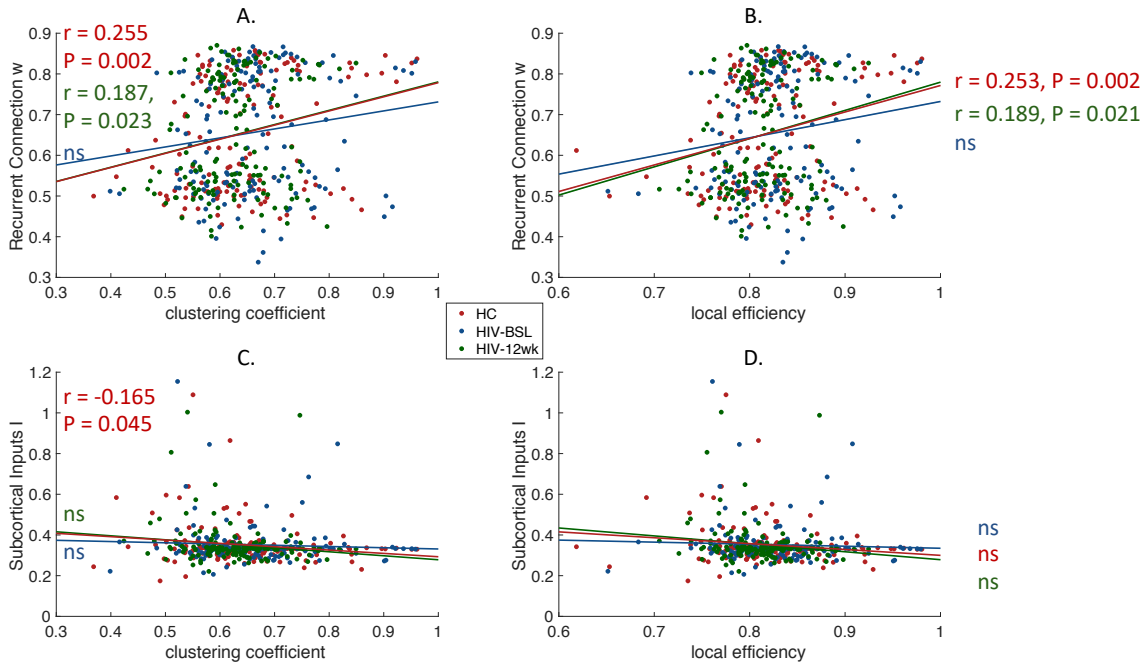

Supplementary Fig. 13. The recurrent connection *w* and subcortical inputs *I* correlated with empirical local network topology using Destrieux atlas. (A) Association between clustering

coefficient and recurrent connection strength w. (B) Association between local efficiency and recurrent connection strength w. (C) Association between clustering coefficient and subcortical inputs I. (D) Association between local efficiency and subcortical inputs I. Red: HC, Blue: HIV+BSL, Green: HIV+12wk. ns: not significant

Reference:

Buxton RB, Wong EC, Frank LR. Dynamics of blood flow and oxygenation changes during brain activation: the balloon model. Magn Reson Med 1998; 39(6): 855-64.

Deco G, Jirsa VK. Ongoing Cortical Activity at Rest: Criticality, Multistability, and Ghost Attractors. Journal of Neuroscience 2012; 32(10): 3366-75.

Deco G, Ponce-Alvarez A, Mantini D, Romani GL, Hagmann P, Corbetta M. Resting-state functional connectivity emerges from structurally and dynamically shaped slow linear fluctuations. J Neurosci 2013; 33(27): 11239-52.

Friston KJ, Harrison L, Penny W. Dynamic causal modelling. Neuroimage 2003; 19(4): 1273-302.

Friston KJ, Mechelli A, Turner R, Price CJ. Nonlinear responses in fMRI: the Balloon model, Volterra kernels, and other hemodynamics. Neuroimage 2000; 12(4): 466-77.

Grubb RL, Jr., Raichle ME, Eichling JO, Ter-Pogossian MM. The effects of changes in PaCO2 on cerebral blood volume, blood flow, and vascular mean transit time. Stroke 1974; 5(5): 630-9.

Heinzle J, Koopmans PJ, den Ouden HEM, Raman S, Stephan KE. A hemodynamic model for layered BOLD signals. Neuroimage 2016; 125: 556-70.

Humphries MD, Gurney K. Network 'small-world-ness': a quantitative method for determining canonical network equivalence. PLoS One 2008; 3(4): e0002051.

Jenkinson M, Bannister P, Brady M, Smith S. Improved optimization for the robust and accurate linear registration and motion correction of brain images. Neuroimage 2002; 17(2): 825-41.

Jenkinson M, Beckmann CF, Behrens TE, Woolrich MW, Smith SM. Fsl. Neuroimage 2012; 62(2): 782-90.

Latora V, Marchiori M. Efficient behavior of small-world networks. Phys Rev Lett 2001; 87(19): 198701.

Rubinov M, Sporns O. Complex network measures of brain connectivity: uses and interpretations. Neuroimage 2010; 52(3): 1059-69.
Schirner M, McIntosh AR, Jirsa V, Deco G, Ritter P. Inferring multi-scale neural mechanisms with brain network modelling. Elife 2018; 7: e28927.
Smith SM. Fast robust automated brain extraction. Hum Brain Mapp 2002; 17(3): 143-55.
Stephan KE, Weiskopf N, Drysdale PM, Robinson PA, Friston KJ. Comparing hemodynamic models with DCM. Neuroimage 2007; 38(3): 387-401.
Watts DJ, Strogatz SH. Collective dynamics of 'small-world' networks. Nature 1998; 393(6684): 440-2.
Wong KF, Wang XJ. A recurrent network mechanism of time integration in perceptual decisions. J Neurosci 2006; 26(4): 1314-28.